Author(s): Alhilaly, Mohammad J.; Bootharaju, Megalamane S.; Joshi, Chakra P; Besong, Tabot M.D.; Emwas, Abdul-Hamid; Mosqueda, Rosalba Juarez; Kaappa, Sami; Malola, Sami; Adil, Karim; Shkurenko, Aleksander; Häkkinen, Hannu; Eddaoudi, Mohamed; Bakr, Osman M.

Title: [Ag67(SPhMe2)32(PPh3)8]3+: Synthesis, Total Structure, and Optical Properties of a Large Box-Shaped Silver Nanocluster

Year: 2016

Version:

Article

[Ag67(SPhMe2)32(PPh3)8]3+: Synthesis, Total Structure, and Optical Properties of a Large Box-Shaped Silver Nanocluster

Mohammad J. Alhilaly, Megalamane S. Bootharaju, Chakra P Joshi, Tabot M.D. Besong, Abdul-Hamid Emwas, Rosalba Juarez Mosqueda, Sami Kaappa, Sami Malola, Karim Adil, Aleksander Shkurenko, Hannu Häkkinen, Mohamed Eddaoudi, and Osman M. Bakr

Just Accepted

[Ag₆₇(SPhMe₂)₃₂(PPh₃)₈]³⁺: Synthesis, Total Structure, and Optical Properties of a Large Box-Shaped Silver Nanocluster

$[Ag_{67}(SPhMe_2)_{32}(PPh_3)_8]^{3+}$: Synthesis, Total Structure, and Optical Properties of a Large Box-Shaped Silver Nanocluster

Mohammad J. Alhilaly,[†,‡] Megalamane S. Bootharaju,[†,‡] Chakra P. Joshi,[†] Tabot M. Besong,[†] Abdul-Hamid Emwas,[⊥] Rosalba Juarez-Mosqueda,[§] Sami Kaappa,[§] Sami Malola,[§] Karim Adil,[‖] Aleksander Shkurenko,[‖] Hannu Häkkinen,*,[§] Mohamed Eddaoudi,[‖] and Osman M. Bakr*,[†]

[†]Division of Physical Sciences and Engineering, King Abdullah University of Science and Technology (KAUST), Thuwal 23955-6900, Saudi Arabia

[⊥]Imaging and Characterization Core Lab, King Abdullah University of Science and Technology (KAUST), Thuwal 23955-6900, Saudi Arabia

[§]Departments of Physics and Chemistry, Nanoscience Center, University of Jyväskylä, FI-40014 Jyväskylä, Finland

[‖]Functional Materials Design, Discovery and Development Research Group (FMD3), Advanced Membranes and Porous Materials Center, Division of Physical Sciences and Engineering, King Abdullah University of Science and Technology (KAUST), Thuwal 23955-6900, Saudi Arabia

ABSTRACT: Engineering the surface ligands of metal nanoparticles is critical in designing unique arrangements of metal atoms. Here, we report the synthesis and total structure determination of a large box-shaped Ag_{67} nanocluster (NC) protected by a mixed shell of thiolate (2,4-dimethylbenzenethiolate, $SPhMe_2$) and phosphine (triphenylphosphine, PPh_3) ligands. Single crystal X-ray diffraction (SCXRD) and electrospray ionization mass spectrometry (ESI-MS) revealed the cluster formula to be $[Ag_{67}(SPhMe_2)_{32}(PPh_3)_8]^{3+}$. The crystal structure shows an Ag_{23} metal core covered by a layer of $Ag_{44}S_{32}P_8$ arranged in the shape of a box. The Ag_{23} core was formed through an unprecedented centered cuboctahedron i.e., Ag_{13}, unlike the common centered Ag_{13} icosahedron geometry. Two types of ligand motifs, eight AgS_3P and eight bridging thiols were found to stabilize the whole cluster. The optical spectrum of this NC displayed highly structured multiple absorption peaks. The electronic structure and optical spectrum of Ag_{67} were computed using time-dependent density functional theory (DFT) both for the full cluster $[Ag_{67}(SPhMe_2)_{32}(PPh_3)_8]^{3+}$ and a reduced model $[Ag_{67}(SH)_{32}(PH_3)_8]^{3+}$. The lowest metal-to-metal transitions in the range of 500 to 800 nm could be explained by considering the reduced model that shows almost identical electronic states to 32 free electrons in a jellium box. The successful synthesis of the large box-shaped Ag_{67} NC facilitated by the combined use of phosphine and thiol paves the way for synthesizing other metal clusters with unprecedented shapes by judicious choice of thiols and phosphines.

INTRODUCTION

Noble metal nanoparticles (NPs), especially ones made of gold and silver, have recently garnered significant attention because of the potential applications of their optical and physicochemical properties,[1-3] which led to their use in catalysis,[4,5] bioimaging and biosensing,[6-9] and light energy conversion[10,11]. Unlike plasmonic NPs (average diameter >2 nm), ultrasmall NPs (typically <2 nm) containing a precise number of atoms completely lose their plasmonic features and display molecular properties[12] due to manifestation of discrete energy levels. Such atomically precise metal NPs, where every single atom influences the overall properties, are often protected by a definite number of ligand molecules. These new functional nanomaterials are called nanoclusters (NCs) or nanomolecules.

Among noble metals, a multitude of gold NCs are reported, including Au_{25},[13-16] Au_{38},[17,18] Au_{67},[19] Au_{102},[20,21] and Au_{144},[22-24] and many of them are completely characterized through single crystal X-ray diffraction (SCXRD). In contrast, the exploration of silver NCs is still lagging, mainly due to their instability, resulting in only a few examples of fully characterized silver NCs. Nevertheless, the number of stable atomically monodisperse thiolate-protected silver NCs is rising, having attracted much

research attention with the hope of utilizing them as a viable and cheaper alternative to gold.[25-34]

A key challenge remaining for silver NCs is obtaining highly anisotropic shapes. In gold, NCs of anisotropic shapes were reported through solely thiols[35,36] and co-ligands of phosphines and thiols[37,38]. Such a strategy of co-ligands in sliver has failed to produce analogous results. Zheng and co-workers demonstrated that the use of a phosphine co-ligand, in addition to thiol, could shrink the silver NC size,[39] while the same pure thiol yielded a cluster of increased size[28] under similar reaction conditions. As an example, the ligand, $HSPhF_2$, was shown to produce Ag_{44} NCs[28] when used alone; however, when used in conjunction with a phosphine co-ligand, a smaller Ag_{14} NC was found to be the final product[39]. On the other hand, Bakr *et al.*[33] showed that the use of phosphine does not change the size of the NC, but has a stabilizing effect on the resulting Ag_{29} NC, wherein phosphine was found to increase the cluster's yield and its stability, and aided in the growth of good-quality single crystals of Ag_{29} NC for its structure determination.

In this work, we demonstrate that the use of a phosphine co-ligand with controlled synthetic parameters plays an important role in determining the shape and size of the NC, where we observed —in contrast to previous reports— an increase of the NC size that results in a unique anisotropic shape. Particularly, we synthesized and fully characterized a novel NC of $[Ag_{67}(SPhMe_2)_{32}(PPh_3)_8]^{3+}$ using a one-pot synthetic strategy, in which both thiol and phosphine co-ligands were judiciously chosen to produce this large stable NC of a box-like shape. While the syntheses of Ag NCs with similar or larger sizes have been reported,[40,41] they were plagued by instability issues precluding their structure elucidation and precise molecular formula determination (e.g. restricting the estimation of NCs' formulae to matrix-assisted laser desorption ionization mass spectrometry). Thus the $[Ag_{67}(SPhMe_2)_{32}(PPh_3)_8]^{3+}$ cluster is particularly significant, as it represents the largest known non-superatom Ag NC to-date; its synthesis opens new avenues of tailoring and elucidating the properties of Ag NCs. Unlike most NCs, theoretical modeling of the Ag_{67} structure reveals a free electron count of n = 32 and a lack of an electronically closed shell as a superatom would, which is a result of the cluster's non-spherical shape. Furthermore, the electronic structure is identifiable using a reduced atomistic model $[Ag_{67}(SH)_{32}(PH_3)_8]^{3+}$, which shows delocalized metal-core states akin to 32 electrons in a box-shaped jellium. We demonstrate that our reduced atomistic model yields a good description of the lowest of transitions in the linear optical absorption spectrum.

RESULTS AND DISCUSSION

Synthesis, purification, and crystallization

Synthesis of $[Ag_{67}(SPhMe_2)_{32}(PPh_3)_8]^{3+}$ NCs involves the reaction of sliver nitrate with $HSPhMe_2$ in a MeOH/DCM solvent mixture (see the experimental section for details and Scheme 1 in the Supporting Information (SI)). Later on, triphenylphosphine (PPh_3) was introduced into the reaction mixture under vigorous stirring to form Ag-thiolate-phosphine complexes. Subsequently, these complexes were reduced using $NaBH_4$ to produce Ag NCs. After completion of the reaction, the NC product was washed with MeOH. The UV-vis absorption spectrum of the as-prepared or raw product showed a novel spectrum (Figure S1A) with optical features completely different from those of Ag_{25} and its doped clusters,[26,42,43] despite the use of same thiol. The photoluminescence (PL) spectrum of the same raw product showed a weak emission at ~820 nm (Figure S2). Interestingly, electrospray ionization mass spectrometry (ESI-MS) of this raw product, and also the singly-washed sample, revealed both $[Ag_{25}(SPhMe_2)_{18}]^-$ and $[Ag_{67}(SPhMe_2)_{32}(PPh_3)_8]^{3+}$ NCs in negative and positive-ion modes, respectively (Figure S3A and B). However, we found that the room-temperature aging of the singly-washed raw product (i.e., the product after the first MeOH-wash) changes color from reddish brown to greenish brown (insets of Figure S1). This greenish brown product was extracted with MeOH, cleaned and redissolved in DCM, and referred to as the 'purified' or the 'final' product (inset of Figure 1). The UV-vis spectrum of this solution consists of strong and well-defined multiple absorption bands in the visible range (Figure 1), which is strikingly different from that of the as-prepared cluster product (Figure S1A). The convergence and sharpening of the features

in the UV-vis spectrum of the final product are indicative of an improvement in the monodispersity of the NCs.
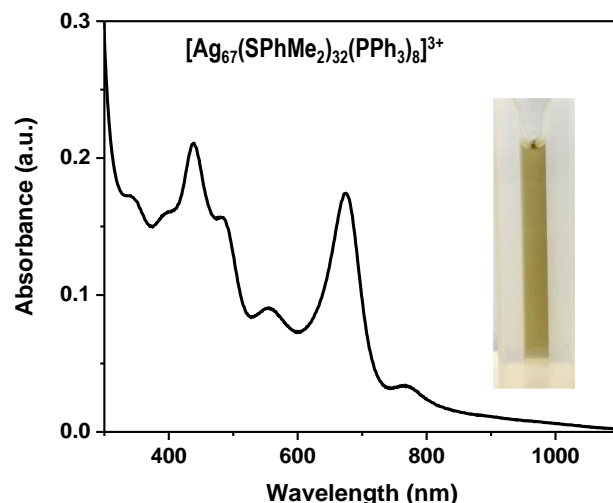
Figure 1. UV-vis absorption spectrum of the purified Ag_{67} NCs in DCM. Inset is a photograph of the purified final product of Ag_{67} NCs.

The ESI-MS of the purified product showed the absence of Ag_{25} (Figure S3C), while only a predominant peak at *m/z* ~4571.87 corresponding to $[Ag_{67}(SPhMe_2)_{32}(PPh_3)_8]^{3+}$ cluster was observed (Figure 2). The absence of Ag_{25} after aging is attributed to its decomposition or conversion to Ag_{67} as Ag_{25} is unstable under ambient conditions for more than a day. The sole charge-state 3+ of Ag_{67} NCs was confirmed from a characteristic peak separation of *m/z* 0.33. The molecular formula of $[Ag_{67}(SPhMe_2)_{32}(PPh_3)_8]^{3+}$ NCs was validated by matching the experimental isotopic pattern with their simulated spectrum (inset of Figure 2), consistent with SCXRD (*vide infra*). It is worth noting that the number of phosphine (PPh_3) ligands in the mass spectrum of Ag_{67} NCs is sensitive to instrumental parameters (see the SI for details). Under soft conditions, the peak for $[Ag_{67}(SPhMe_2)_{32}(PPh_3)_8]^{3+}$ was predominant, while at moderately harsh conditions, cluster peaks with sequentially-lost PPh_3 were more noticeable (Figure S3). Consequently, a series of nine peaks of $[Ag_{67}(SPhMe_2)_{32}(PPh_3)_x]^{3+}$ could be observed, corresponding to x = 0-8, where the difference (*m/z* ~87) between every two adjacent peaks was one PPh_3 (Figure S3). The loss of PPh_3 ligands during the electrospray ionization is likely due to the weak bonding of the phosphine ligands to the Ag_{67} NCs, as it was also noted in other Ag and doped clusters.[33,44]

2
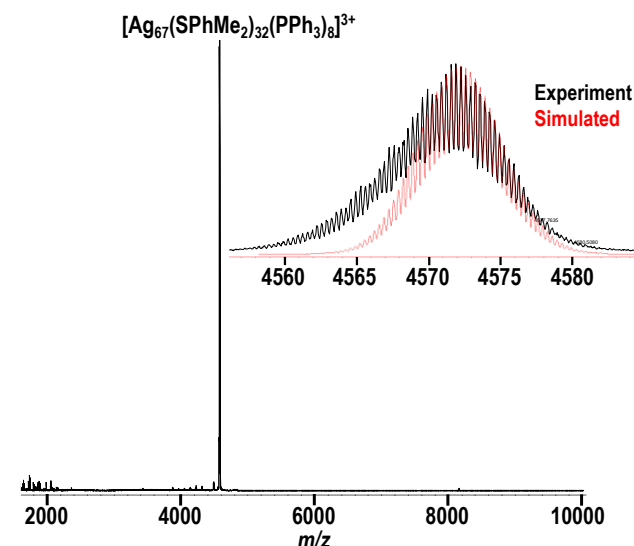
Figure 2. Positive mode ESI-MS of purified $[Ag_{67}(SPhMe_2)_{32}(PPh_3)_8]^{3+}$ NC in DCM. The inset shows a matching of isotope patterns between the experimental and simulated spectra.

To further confirm the purity and monodispersity of the final Ag_{67} NCs, analytical ultracentrifugation (AUC) was performed. The AUC results show that Ag_{67} displays a high degree of monodispersity in DCM as seen by the 3D representation of sedimentation (s) and diffusion (D) coefficient distributions (Figure S4). Also, the near vertical plot of the van Holde-Weichet (vHW) analysis is a distinguishing feature of monodisperse systems (Figure S5). Polydisperse systems usually show a slanting non-vertical vHW profile of the sedimentation coefficient distributions. Ag_{67} has a standard sedimentation coefficient of 3.0S (or 3.0 x 10^{-13}s), within the range observed for other silver NCs.[30,31]

^{31}P and ^1H nuclear magnetic resonance (NMR) spectroscopy was used to probe the chemical composition and the ligand environments of Ag_{67} NCs. The ^1H NMR (Figure S6) shows different peaks at the aromatic and aliphatic regions. The broad peaks in the aromatic region between 6.8-7.3 ppm are associated with the aromatic protons of $SPhMe_2$ ligands, while the three peaks between 7.3-7.6 ppm are corresponding to the aromatic protons of PPh_3. In agreement with published reports,[45] the spectra show different peaks between 0.75-2.5 ppm related to the methyl group (CH_3) of $SPhMe_2$ (Figure S6B). Different chemical shifts of CH_3 confirmed different chemical environments of various methyl groups within the $[Ag_{67}(SPhMe_2)_{32}(PPh_3)_8]^{3+}$ NC. Figure S7 shows the ^{31}P NMR peaks of the clusters in comparison to ^{31}P NMR peak of free PPh_3. A broad peak of the cluster at 8.1 ppm is due to the phosphine bound to the cluster, while a sharp peak at 27.4 ppm could be due to free triphenylphosphine oxide (PPh_3O), probably resulted from the oxidation of free PPh_3 (if anything left in the solution during washing steps).

Clearly, the aging, or size-focusing step, is essential to concentrate the final product of Ag_{67} as it allows the separation and precipitation of unstable species (Ag_{25}) spontaneously. The selective formation of Ag_{67} as the final product over Ag_{25} or other size clusters may be due to its thermodynamic and geometric

stability (*vide infra*), which was gained by the unique combination of Ag, PPh_3 and $HSPhMe_2$. The final Ag_{67} NCs was found to be compatible with MeOH and 1-propanol in addition to DCM, as its UV-vis features were appeared consistently in these solvents (Figure S8A). Furthermore, the Ag_{67} was found to be stable at 5 °C in DCM for at least five days (Figure S8B). However, unlike Ag_{25},[26] the purified Ag_{67} NCs were found not to luminesce (Figure S2). The emission peak of the as-prepared product was most likely due to the presence of Ag_{25}. This fact was further confirmed by PL measurements of a mixture of pure Ag_{25} and Ag_{67}, where the emission peak appeared at the position of as-prepared Ag_{67} product and also pure Ag_{25} (Figure S2). The yield of the final Ag_{67} NCs was ~25% (based on Ag atom content).

**X-ray Crystal Structure**

Single crystal X-ray diffraction (SCXRD) measurements were applied to single crystals that were grown at 4 °C by layering hexane onto a DCM solution of freshly purified Ag_{67} NCs. The crystal data analysis shows that the overall composition of NCs is $Ag_{67}(SPhMe_2)_{32}(PPh_3)_8$, which is consistent with the ESI-MS formula. The Ag_{67} NC crystallizes into an orthorhombic crystal system (space group *Ccc*2), see the SI for details of the crystal data and the refinement.

The total structure of Ag_{67} is shown in Figure S9. The packing structure clearly reveals the location of two $[BPh_4]^-$ ions per cluster, while it was difficult to localize the third counterion, which is most probably disordered in the cavities. However, the sole 3+ charge-state is evident from ESI-MS and DFT (*vide infra*). The total structure of Ag_{67} without hydrogens and counterions is shown in Figure 3A. For clarity, all the carbon atoms are omitted in Figure 3B, which shows a box-shape of the $Ag_{67}S_{32}P_8$. The dissection of $Ag_{67}S_{32}P_8$ was conducted based on the connectivity of metal atoms to ligands (both thiols and phosphines). The metal structure that is not connected to ligands is shown in Figure 3C. It consists of 23 Ag atoms in a box-shape. The remaining $Ag_{44}(SPhMe_2)_{32}(PPh_3)_8$ framework (Figure 3D) acts as a closed metal-ligand protecting layer that encapsulates the Ag_{23} core.

The formation of the Ag_{23} core is illustrated in Figure S10. Ag_{23} consists of a centered Ag_{13} cuboctahedron – a core shape seldom observed in thiol- and phosphine-protected silver NCs (Figure S10A). Usually in Ag NCs, centered[26,33] and non-centered icosahedra[28,29] are the archetypal core-shapes. Two opposite square faces of Ag_{13} are shared (Figure S10B) with two Ag_8 crowns to form an Ag_{21} unit as in Figure S10C. Finally, the two open crown positions are closed by two silver atoms to form the Ag_{23} structure as in Figure S10D (the slight rotation of the structure of Figure S10D gives the Figure S10E). This crowning of the Ag_{13} cuboctahedron leads to the growth of Ag_{67} cluster in a box-shape. The average Ag-Ag distance from the central atom to cuboctahedron atoms and between cuboctahedron atoms of Ag_{13} are 2.860 and 2.860 Å, respectively, comparable to the Ag-Ag bond length 2.88 Å in bulk silver, indicating the strong interaction among the Ag_{13} core atoms. Notably, the $Ag_{cuboctahedron}$-Ag_{crown} and $Ag_{cuboctahedron}$-$Ag_{crown-center}$ distances are 2.806 and 2.910 Å, respectively. The large bond distance of $Ag_{cuboctahedron}$-$Ag_{crown-center}$ and the resultant relatively less interactions among these Ag atoms inclines the growth of cluster towards a box-shape.

3
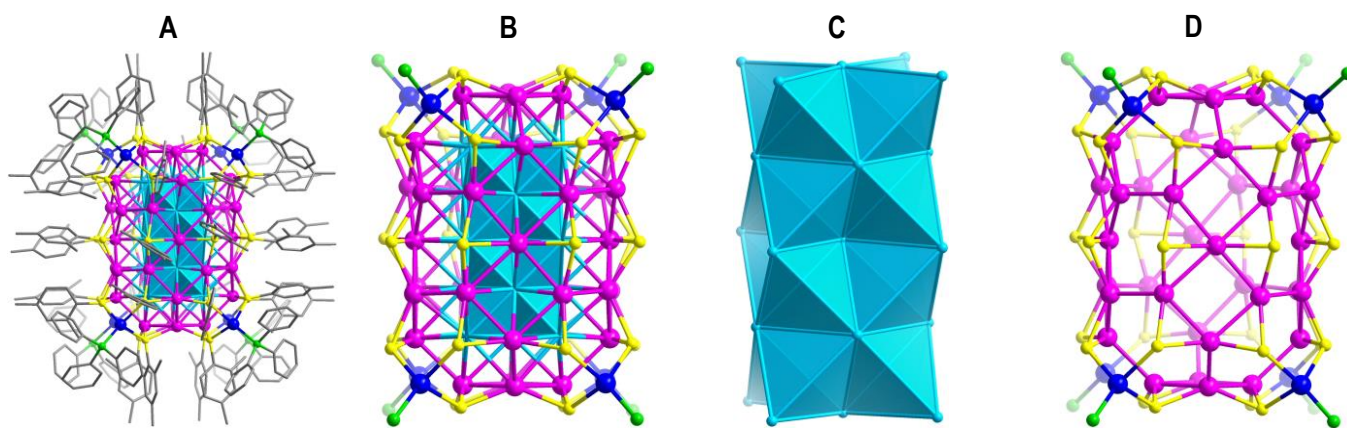
Figure 3. (A) Total structure of $[Ag_{67}(SPhMe_2)_{32}(PPh_3)_8]^{3+}$ NC. (B) The structure of $Ag_{67}S_{32}P_8$ obtained by disconnecting carbon atoms in A. (C) Ag_{23} metal core. (D) The structure of the NC without Ag_{23} metal core i.e., $Ag_{44}(SPhMe_2)_{32}(PPh_3)_8$. Color legends: gray, carbon; blue, magenta, and cyan, silver; yellow, sulfur; green, phosphorous. Hydrogen atoms are omitted for simplicity.

The formation of the $Ag_{44}(SPhMe_2)_{32}(PPh_3)_8$ metal-ligand encapsulating layer starts from a closed Ag_{36} cuboid-like box (Figure S11A). The structure of Ag_{36} has eight planar hexagons, ten planar squares and four non-planar hexagons. The Ag-Ag bond distance range in this Ag_{36} metal layer is 2.846-3.048 Å, with an average of 2.9195 Å. Note that four non-planar hexagons are located at the central part of Ag_{36}. Out of six Ag atoms of a non-planar hexagon, four Ag atoms are in one plane, away from Ag_{23} core, while the remaining two Ag atoms are in a different plane, towards the Ag_{23} core. Each sulfur atom (at the central part of the Ag_{36}) of a thiol connects to three Ag atoms of a non-planar hexagon (Figure S11B). In total, two bridging thiols[46,47] are present per every non-planar hexagon. Therefore, four non-planar hexagons have eight bridging sulfurs to form the structure of $Ag_{36}S_8$ (Figure S11B). In addition to this simple bridging thiol motif-type, there is another type of ligand motif, AgS_3P. As mentioned earlier that there are eight planar hexagons. Each sulfur of the AgS_3P motif bridges the two adjacent Ag atoms of a planar hexagon. In other words, one AgS_3P motif is completely bound to single planar hexagon. Therefore, eight AgS_3P motifs cover the eight planar hexagons to form a metal-ligand layer structure of $Ag_{44}S_{32}P_8$ (Figure S11C). Encapsulation of Ag_{23} core by $Ag_{44}S_{32}P_8$ layer gives the total structure of $Ag_{67}S_{32}P_8$ (Figure 3B). After encapsulation of Ag_{23} core in $Ag_{44}S_{32}P_8$ layer, all the four crown Ag atoms (top Ag atoms) of a crown of Ag_{23} core are positioned at the centers of four planar hexagons of Ag_{36}. The crown-closing Ag atom of the same crown is connected to a planar square face at one extreme of the Ag_{36} cuboid-like box. Similarly, the remainder five Ag atoms of other bottom crown are positioned at the other extreme of the Ag_{36} box and the Ag_{13} cuboctahedron is positioned at the center of Ag_{36} box.

Alternatively, the $Ag_{44}S_{32}P_8$ metal-ligand layer can also be viewed as follows. There are two Ag_{16} units (Figure S12A), each look like a bowl. Each bowl has four planar hexagons and a planar square as the base. These two bowls are joined (from open side) by four one-dimensional S-Ag-S (average Ag-S distance = 2.619 Å) motifs (Figure S12B) to form $Ag_{36}S_8$ (Figure S12C). This $Ag_{36}S_8$ is exactly the same as in Figure S11B. Subsequently, eight three-dimensional AgS_3P motifs cover eight planar hexagons to produce $Ag_{44}S_{32}P_8$ (Figure S12E). This $Ag_{44}S_{32}P_8$ scaffolding accommodates the Ag_{23} core as described before to form the total structure of $Ag_{67}S_{32}P_8$ (Figure S12F,G).

Theoretical analysis of the electronic structure

The electronic structure of the $[Ag_{67}(SPhMe_2)_{32}(PPh_3)_8]^{3+}$ cluster was analyzed by using the experimental crystal structure and also by building a reduced model cluster $[Ag_{67}(SH)_{32}(PH_3)_8]^{3+}$. In that model, positions of Ag, S, and P atoms were fixed to experimental crystal coordinates (as shown in Figure 3B) and S-H and P-H bonds were relaxed to equilibrium. The electronic structure was solved by using the density functional theory (DFT) implemented in the real-space code GPAW.[48] The electronic exchange-correlation interaction was described by the PBE functional.[49]

We found that the $[Ag_{67}(SPhMe_2)_{32}(PPh_3)_8]^{3+}$ cluster has an appreciable energy gap, about 0.36 eV, between the highest occupied (HOMO) and lowest unoccupied (LUMO) molecular orbitals, rendering the cluster electronically stable (the reduced model cluster has a similar gap of 0.43 eV). Visual inspection of several of the silver-based Kohn-Sham molecular orbitals of the $[Ag_{67}(SH)_{32}(PH_3)_8]^{3+}$ model in the region of the HOMO-LUMO gap showed remarkable similarity to box-like quantum states in the jellium model, where each state could be labeled with (n_x, n_y, n_z) triplets giving the number of nodes in x-, y-, and z-directions, respectively. By employing the widely-used rule[50] to count the "free electrons" (Ag(5s) electrons that are not needed for stabilization of the ligand layer) in the metal core, one gets 67-32-3 = 32 free electrons. In fact, state symmetries and their energy order in $[Ag_{67}(SH)_{32}(PH_3)_8]^{3+}$ were identical to states of 32 electrons in a jellium box, where the background charge was set to +12 to mimic the approximate total of Bader charges of all silver atoms in the $[Ag_{67}(SH)_{32}(PH_3)_8]^{3+}$ model cluster (the details of this analysis is a subject of a follow-up theoretical paper).

4

A

B
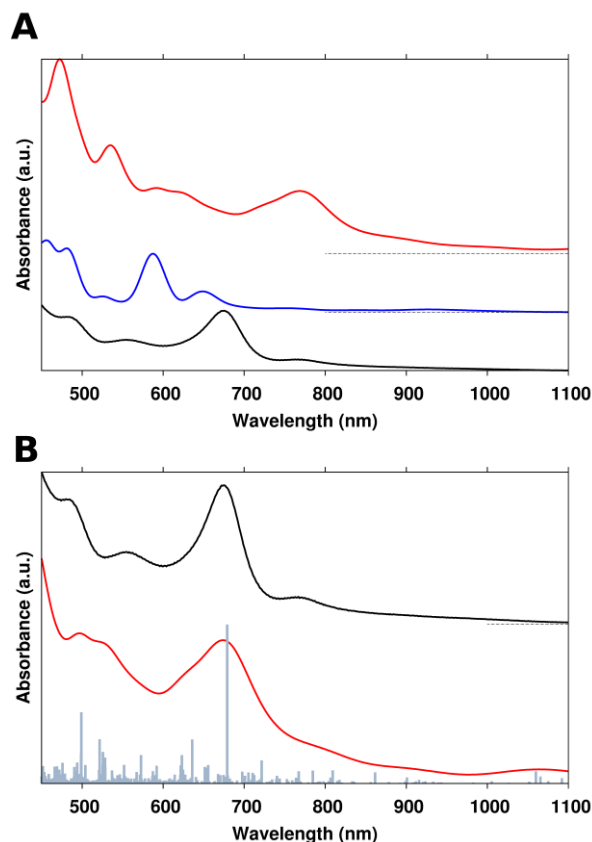
Figure 4. (A) Computed optical absorption spectra of the cluster [Ag₆₇(SPhMe₂)₃₂(PPh₃)₈]³⁺ (red) and the model cluster [Ag₆₇(SH)₃₂(PH₃)₈]³⁺ (blue) as compared to the experimental data (black). (B) The computed spectrum of [Ag₆₇(SPhMe₂)₃₂(PPh₃)₈]³⁺ blue-shifted by 95 nm (red) compared to the experiment (black). Gray sticks show the individual transitions (delta-function-like peaks showing the relative oscillator strengths). The continuous computational spectra are sums of Gaussian smoothed individual transitions (width of 0.05 eV). The intensity of the computational spectra is scaled so that the dominant peaks are approximately of similar intensity.

We calculated the optical absorption spectrum of both the [Ag₆₇(SPhMe₂)₃₂(PPh₃)₈]³⁺ cluster and the [Ag₆₇(SH)₃₂(PH₃)₈]³⁺ model cluster by using DFT in the linear-response formalism as implemented in GPAW.[51] The PBE functional was used for calculating the oscillator matrix. Figure 4 shows that both calculations reproduce the shape of the lower-energy part of the calculated spectrum very well with the experimental data, albeit a slight blue-shift of about 87 nm for [Ag₆₇(SH)₃₂(PH₃)₈]³⁺ and 95 nm red-shift of the full cluster [Ag₆₇(SPhMe₂)₃₂(PPh₃)₈]³⁺. This red-shift could be expected to arise from the chosen PBE functional. The observed blue-shift for [Ag₆₇(SH)₃₂(PH₃)₈]³⁺ model is caused by the lack of the true ligand layer around the metal core, thus resulting in a slightly modified (compressed) electron density in the core that shifts all the transitions to blue. Analysis of the lowest metal-to-metal transitions for the [Ag₆₇(SH)₃₂(PH₃)₈]³⁺ model showed that they arise from contributions from Kohn-Sham states where the total number of nodes ($n_x + n_y + n_z$) changed by ± 1, thus confirming the dipole selection rule in a quantum box.

CONCLUSION

In conclusion, we report the synthesis and total structure of a new silver NC of [Ag₆₇(SPhMe₂)₃₂(PPh₃)₈]³⁺ using SCXRD, DFT, ESI-MS, and NMR. The combined use of thiol and phosphine ligands in our study demonstrates that silver clusters can be made in stable non-spherical box-like shapes, in sharp contrast to previously reported Ag₄₄ and related "superatoms" that have an approximate spherical core. The optical absorption spectrum of Ag₆₇ NC shows distinct optical features, and the theoretical calculations reveal that the lowest optical transitions can be understood by invoking delocalized electronic states in a quantum box. This achievement will push the limit of synthesizing large silver NCs with high-stability and previously unknown shapes providing a new degree of freedom in tailoring their properties.

EXPERIMENTAL SECTION

Materials. All the following chemicals and solvents were purchased and used without further purification. Silver nitrate (AgNO₃, 99%, Aldrich), 2,4-dimethylbenzenethiol (HSPhMe₂, Alfa Aesar), triphenylphosphine (PPh₃, 99%, Aldrich), sodium borohydride (NaBH₄, 99.99%, Aldrich), sodium tetraphenylborate (NaBPh₄, Aldrich). Dichloromethane (DCM, HPLC grade), methanol (MeOH, HPLC grade) and ethanol (EtOH, HPLC grade, 99.9%) were purchased from Sigma Aldrich. Distilled water (18.2 MΩcm) was collected from Milli-Q (Millipore, 0.22 µm) machine.

Synthesis and purification of [Ag₆₇(SPhMe₂)₃₂(PPh₃)₈]³⁺ NCs. In a glass vial, 40 mg of AgNO₃ was completely dissolved in 5 mL of MeOH by sonication. Then, 10 mL of DCM that containing 40 µL of HSPhMe₂ was added to the reaction vial. The reaction mixture was vigorously stirred inside a fume hood at room temperature (25 °C) that produced a turbid yellow mixture. After 20 min. of stirring, 200 mg of PPh₃ dissolved in 2 mL of DCM was immediately added to the reaction solution. The turbid yellow mixture turned to a clear colorless solution. After that, 500 µL of an aqueous solution of NaBH₄ (42 mg, 1.11 mmol of NaBH₄ dissolved in 2 mL H₂O) was added drop-wise to the solution producing a dark solution, which was allowed to react at 1200 rpm for 2 h.

The dark as-prepared solution was first centrifuged at 8000 rpm for 5 min. to get rid of any insoluble byproducts. The solution was then evaporated to decrease the solution volume to 10 mL, and then MeOH was added to precipitate the NCs followed by centrifugation (8000 rpm/ 5 min.). The obtained precipitate was dissolved in 5 mL of DCM, while the supernatant was discarded. After first wash, i.e., the sample now in DCM was aged overnight at 25 °C under ambient conditions. During the aging time, the sample color slowly started changing from reddish brown to greenish brown/olive. In the next day, the sample was dried and the precipitate was extracted with MeOH, and then centrifuged (8000 rpm for 5 min.) to eliminate insoluble species. The solution of NCs in MeOH was again aged at 25 °C for few hours such that during the time of aging, the sample showed orange/pink junk precipitates which can be removed by centrifugation (8000 rpm for 5 min.). Using a rotary evaporator, the sample was dried. The purified NCs were dissolved in ~2 mL of DCM. The final product of Ag₆₇ NCs solution was allowed to react with NaBPh₄ (which had an equal molar of AgNO₃) to further stabilize the clusters, [Ag₆₇(SPhMe₂)₃₂(PPh₃)₈]³⁺. This stabilized final product was stored in a tightly capped vial inside the fridge (4 °C) to obtain single crystals (see below).

Crystallization. A very concentrated DCM solution (~8-10 mg/mL) of Ag₆₇ NCs was taken from the original purified solution into a small clean NMR tube after filtration using a syringe filter (0.22 µm of pore size). Hexane was layered on the top of DCM solution of NCs and then

5

the cap was closed and stored in a refrigerator at 4 °C. After approximately 3-4 days, black crystals were obtained with the quality suitable for X-ray diffraction (Figure S13).

ASSOCIATED CONTENT

Supporting Information. Instrumentation, Ag_{67} synthesis scheme, UV-vis, PL emission, ESI-MS, AUC, ^{1}H NMR and ^{31}P NMR spectra, and crystal structure analysis of Ag_{67}. The Supporting Information is available free of charge on the ACS publication website at DOI: .

AUTHOR INFORMATION

Corresponding Author

*osman.bakr@kaust.edu.sa & hannu.j.hakkinen@jyu.fi

Notes

The authors declare no competing financial interest.

Author Contributions

‡These authors contributed equally.

ACKNOWLEDGMENT

REFERENCES

(1) Joshi, C. P.; Bootharaju, M. S.; Bakr, O. M. *J. Phys. Chem. Lett.* **2015**, *6*, 3023.

(2) Jin, R. *Nanoscale* **2015**, *7*, 1549.

(3) Tsukuda, T.; Häkkinen, H. Protected Metal Clusters: From Fundamentals to Applications; Elsevier Science, 2015.

(4) Negishi, Y.; Mizuno, M.; Hirayama, M.; Omatoi, M.; Takayama, T.; Iwase, A.; Kudo, A. *Nanoscale* **2013**, *5*, 7188.

(5) Urushizaki, M.; Kitazawa, H.; Takano, S.; Takahata, R.; Yamazoe, S.; Tsukuda, T. *J. Phys. Chem. C* **2015**, *119*, 27483.

(6) Tao, Y.; Li, M.; Ren, J.; Qu, X. *Chem. Soc. Rev.* **2015**, *44*, 8636.

(7) Obliosca, J.; Liu, C.; Batson, R.; Babin, M.; Werner, J.; Yeh, H.-C. *Biosensors* **2013**, *3*, 185.

(8) Kwak, K.; Kumar, S. S.; Pyo, K.; Lee, D. *ACS Nano* **2014**, *8*, 671.

(9) Zheng, K.; Yuan, X.; Goswami, N.; Zhang, Q.; Xie, J. *RSC Adv.* **2014**, *4*, 60581.

(10) Chen, Y.-S.; Choi, H.; Kamat, P. V. *J. Am. Chem. Soc.* **2013**, *135*, 8822.

(11) Stamplecoskie, K. G.; Swint, A. *J. Mater. Chem. A* **2016**, *4*, 2075.

(12) Cathcart, N.; Mistry, P.; Makra, C.; Pietrobon, B.; Coombs, N.; Jelokhani-Niaraki, M.; Kitaev, V. *Langmuir* **2009**, *25*, 5840.

(13) Heaven, M. W.; Dass, A.; White, P. S.; Holt, K. M.; Murray, R. W. *J. Am. Chem. Soc.* **2008**, *130*, 3754.

(14) Zhu, M.; Aikens, C. M.; Hollander, F. J.; Schatz, G. C.; Jin, R. *J. Am. Chem. Soc.* **2008**, *130*, 5883.

(15) Akola, J.; Walter, M.; Whetten, R. L.; Häkkinen, H.; Grönbeck, H. *J. Am. Chem. Soc.* **2008**, *130*, 3756.

(16) Ouyang, R.; Jiang, D.-e. *J. Phys. Chem. C* **2015**, *119*, 21555.

(17) Qian, H.; Eckenhoff, W. T.; Zhu, Y.; Pintauer, T.; Jin, R. *J. Am. Chem. Soc.* **2010**, *132*, 8280.

(18) Fernando, A.; Aikens, C. M. *J. Phys. Chem. C* **2016**, *120*, 14948.

(19) Nimmala, P. R.; Yoon, B.; Whetten, R. L.; Landman, U.; Dass, A. *J. Phys. Chem. A* **2013**, *117*, 504.

(20) Jadzinsky, P. D.; Calero, G.; Ackerson, C. J.; Bushnell, D. A.; Kornberg, R. D. *Science* **2007**, *318*, 430.

(21) Salorinne, K.; Malola, S.; Wong, O. A.; Rithner, C. D.; Chen, X.; Ackerson, C. J.; Hakkinen, H. *Nat. Commun.* **2016**, *7*, 10401.

(22) Qian, H.; Jin, R. *Chem. Mater.* **2011**, *23*, 2209.

(23) Qian, H.; Jin, R. *Nano Lett.* **2009**, *9*, 4083.

(24) Chaki, N. K.; Negishi, Y.; Tsunoyama, H.; Shichibu, Y.; Tsukuda, T. *J. Am. Chem. Soc.* **2008**, *130*, 8608.

(25) Dhayal, R. S.; Liao, J.-H.; Liu, Y.-C.; Chiang, M.-H.; Kahlal, S.; Saillard, J.-Y.; Liu, C. W. *Angew. Chem. Int. Ed.* **2015**, *54*, 3702.

(26) Joshi, C. P.; Bootharaju, M. S.; Alhilaly, M. J.; Bakr, O. M. *J. Am. Chem. Soc.* **2015**, *137*, 11578.

(27) Bootharaju, M. S.; Joshi, C. P.; Alhilaly, M. J.; Bakr, O. M. *Chem. Mater.* **2016**, *28*, 3292.

(28) Yang, H.; Wang, Y.; Huang, H.; Gell, L.; Lehtovaara, L.; Malola, S.; Häkkinen, H.; Zheng, N. *Nat. Commun.* **2013**, *4*, 2422.

(29) Desireddy, A.; Conn, B. E.; Guo, J.; Yoon, B.; Barnett, R. N.; Monahan, B. M.; Kirschbaum, K.; Griffith, W. P.; Whetten, R. L.; Landman, U.; Bigioni, T. P. *Nature* **2013**, *501*, 399.

(30) AbdulHalim, L. G.; Ashraf, S.; Katsiev, K.; Kirmani, A. R.; Kothalawala, N.; Anjum, D. H.; Abbas, S.; Amassian, A.; Stellacci, F.; Dass, A.; Hussain, I.; Bakr, O. M. *J. Mater. Chem. A* **2013**, *1*, 10148.

(31) Harkness, K. M.; Tang, Y.; Dass, A.; Pan, J.; Kothalawala, N.; Reddy, V. J.; Cliffel, D. E.; Demeler, B.; Stellacci, F.; Bakr, O. M.; McLean, J. A. *Nanoscale* **2012**, *4*, 4269.

(32) Bakr, O. M.; Amendola, V.; Aikens, C. M.; Wenseleers, W.; Li, R.; Dal Negro, L.; Schatz, G. C.; Stellacci, F. *Angew. Chem.* **2009**, *121*, 6035.

(33) AbdulHalim, L. G.; Bootharaju, M. S.; Tang, Q.; Del Gobbo, S.; AbdulHalim, R. G.; Eddaoudi, M.; Jiang, D.-e.; Bakr, O. M. *J. Am. Chem. Soc.* **2015**, *137*, 11970.

(34) Jin, R.; Zhao, S.; Xing, Y.; Jin, R. *Cryst. Eng. Comm.* **2016**, *18*, 3996.

(35) Zeng, C.; Chen, Y.; Iida, K.; Nobusada, K.; Kirschbaum, K.; Lambright, K. J.; Jin, R. *J. Am. Chem. Soc.* **2016**, *138*, 3950.

(35) Chen, Y.; Zeng, C.; Liu, C.; Kirschbaum, K.; Gayathri, C.; Gil, R. R.; Rosi, N. L.; Jin, R. *J. Am. Chem. Soc.* **2015**, *137*, 10076.

(37) Das, A.; Li, T.; Nobusada, K.; Zeng, Q.; Rosi, N. L.; Jin, R. *J. Am. Chem. Soc.* **2012**, *134*, 20286.

(38) Shichibu, Y.; Negishi, Y.; Watanabe, T.; Chaki, N. K.; Kawaguchi, H.; Tsukuda, T. *J. Phys. Chem. C* **2007**, *111*, 7845.

(39) Yang, H.; Lei, J.; Wu, B.; Wang, Y.; Zhou, M.; Xia, A.; Zheng, L.; Zheng, N. *Chem. Commun.* **2013**, *49*, 300.

(40) Bootharaju, M. S.; Burlakov, V. M.; Besong, T. M. D.; Joshi, C. P.; AbdulHalim, L. G.; Black, D. M.; Whetten, R. L.; Goriely, A.; Bakr, O. M. *Chem. Mater.* **2015**, *27*, 4289.

(41) Chakraborty, I.; Erusappan, J.; Govindarajan, A.; Sugi, K. S.; Udayabhaskararao, T.; Ghosh, A.; Pradeep, T. *Nanoscale* **2014**, *6*, 8024.

(42) Bootharaju, M. S.; Joshi, C. P.; Parida, M. R.; Mohammed, O. F.; Bakr, O. M. *Angew. Chem. Int. Ed.* **2016**, *55*, 922.

(43) Yan, J.; Su, H.; Yang, H.; Malola, S.; Lin, S.; Häkkinen, H.; Zheng, N. *J. Am. Chem. Soc.* **2015**, *137*, 11880.

(44) Soldan, G.; Aljuhani, M. A.; Bootharaju, M. S.; AbdulHalim, L. G.; Parida, M. R.; Emwas, A.-H.; Mohammed, O. F.; Bakr, O. M. *Angew. Chem. Int. Ed.* **2016**, *55*, 5749.

(45) Wang, S.; Jin, S.; Yang, S.; Chen, S.; Song, Y.; Zhang, J.; Zhu, M. *Sci. Adv.* **2015**, *1*, e1500441.

(46) Li, G.; Lei, Z.; Wang, Q.-M. *J. Am. Chem. Soc.* **2010**, *132*, 17678.

(47) Chen, Y.; Liu, C.; Tang, Q.; Zeng, C.; Higaki, T.; Das, A.; Jiang, D.-e.; Rosi, N. L.; Jin, R. *J. Am. Chem. Soc.* **2016**, *138*, 1482.

(48) Enkovaara, J.; Rostgaard, C.; Mortensen, J. J.; Chen, J.; Dułak, M.; Ferrighi, L.; Gavnholt, J.; Glinsvad, C.; Haikola, V.; Hansen, H. A.; Kristoffersen, H. H.; Kuisma, M.; Larsen, A. H.; Lehtovaara, L.; Ljungberg, M.; Lopez-Acevedo, O.; Moses, P. G.; Ojanen, J.; Olsen, T.; Petzold, V.; Romero, N. A.; Stausholm-Møller, J.; Strange, M.; Tritsaris, G. A.; Vanin, M.; Walter, M.; Hammer, B.; Häkkinen, H.; Madsen, G. K. H.; Nieminen, R. M.; Nørskov, J. K.; Puska, M.; Rantala, T. T.; Schiøtz, J.; Thygesen, K. S.; Jacobsen, K. W. *J. Phys. Condens. Matter.* **2010**, *22*, 253202.

(49) Perdew, J. P.; Burke, K.; Ernzerhof, M. *Phys. Rev. Lett.* **1996**, *77*, 3865.

6

(50) Walter, M.; Akola, J.; Lopez-Acevedo, O.; Jadzinsky, P. D.; Calero, G.; Ackerson, C. J.; Whetten, R. L.; Grönbeck, H.; Häkkinen, H. *Proc. Natl. Acad. Sci.* **2008**, *105*, 9157.
(51) Walter, M.; Häkkinen, H.; Lehtovaara, L.; Puska, M.; Enkovaara, J.; Rostgaard, C.; Mortensen, J. J. *J. Chem. Phys.* **2008**, *128*, 244101.

Table of Contents